Article

Statistical Physics Model of Seismic Activation Preceding a Major Earthquake

Daniel Brox †

† Affiliation; brox@alumni.caltech.edu

Abstract: Starting from earthquake fault dynamic equations, a correspondence between earthquake occurrence statistics in a seismic region before a major earthquake and eigenvalue statistics of a differential operator whose bound state eigenfunctions characterize the distribution of stress in the seismic region is derived. Modeling these eigenvalue statistics with a 2D Coulomb Gas statistical physics model, previously reported deviation of seismic activation earthquake occurence statistics from Gutenberg-Richter statistics in time intervals preceding the major earthquake is derived. It is also explained how statistical physics modelling predicts a finite dimensional nonlinear dynamic system describes real time velocity model evolution in the region undergoing seismic activation, and how this prediction can be tested experimentally.

Keywords: seismic;activation;statistical;physics

Citation: Brox, D. Statistical Physics Model of Seismic Activation Preceding a Major Earthquake. *Journal Not Specified* **2024**, *1*, 0. https://doi.org/

Received:
Revised:
Accepted:
Published:

1. Introduction

An increase in the number of intermediate sized earthquakes (M > 3.5) in a seismic region preceding the occurrence of a major earthquake ($7 <$ M < 8), referred to as seismic activation, has been observed to occur before many major earthquakes [5]. For example, seismic activation was observed in a geographic region spanning $34^\circ N - 38^\circ N \times 20^\circ E - 27^\circ E \approx 444km\times$630km for a period of time between January 1, 1966 and April 10, 2002 [38]. Figure 1 shows a schematic plot of the cumulative distribution of earthquakes of different magnitudes in a region undergoing seismic activation in two different time intervals of equal duration preceding occurrence of a major earthquake at time $\tau = \tau_0$, where τ is a real time parameter and τ_0 is the time of major earthquake occurrence [30]. Importantly, the cumulative distribution of earthquakes in a time interval of fixed width increasingly deviates away from a Gutenberg-Richter linear log-magnitude plot as the end of the time interval approaches τ_0.

As an alternative to counting earthquakes of different magnitude in different time intervals preceding a major earthquake at time $\tau = \tau_0$, seismic activation has also been quantified as a power law increase in the cumulative Benioff strain $\mathcal{C}(\tau)$ defined as:

$$\mathcal{C}(\tau) = \sum_{i=1}^{n(\tau)} \mathrm{M}_{0,\mathrm{i}}^{1/2}, \tag{1}$$

where $\mathrm{M}_{0,i}$ is the seismic moment of the i^{th} earthquake in the region starting from a time $\tau = 0$ preceding the major earthquake, and $n(\tau)$ is the number of earthquakes occurring in the region up to time τ [27]. For example, it has been put forth that $C(\tau)$ should equate to the power law expression:

$$a - b(\tau_0 - \tau)^\gamma, \tag{2}$$

where $(\tau_0 - \tau)$ is the time to major earthquake occurrence, a is the cumulative Benioff strain at $\tau = \tau_0$, and the constants b and γ are used to fit the formula to measured data [26]. When a fit to real seismic data is performed, a value $\gamma \approx 0.3$ is typical [5].

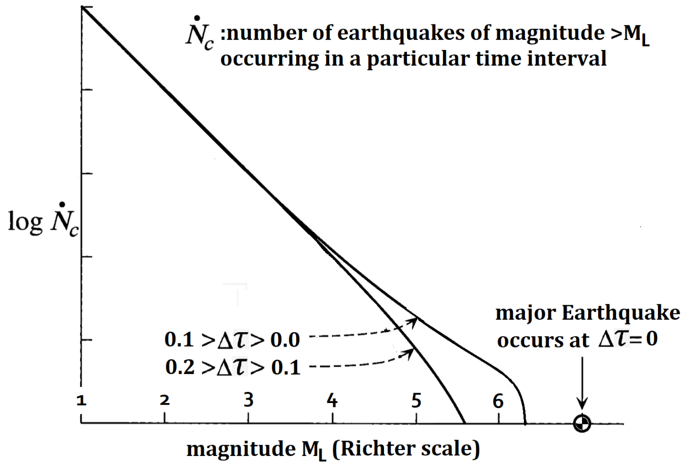

Figure 1. Plot of the cumulative distribution of earthquakes of different magnitudes in a seismic zone in two different time intervals of equal width preceding occurrence of a major earthquake at $\Delta\tau = \tau_0 - \tau = 0$ [30].

A mathematical model of seismic activation based on damage mechanics of earthquake faults has been put forth to account for equation (2) with a value $\gamma = 1/3$ [3]. In this model, cumulative Benioff strain is expressed as a function of the spatial average of a real time varying crack density parameter defined at each location along an earthquake fault. Then, the value $\gamma = 1/3$ is derived by assuming a particular form for the differential equation describing real time evolution of the crack density that derives from a Boltzman kinetic type description of how cracks of different lengths at different positional locations propagate and join together [38].

In addition to the damage mechanics model of seismic activation, an empirical model of seismic activation using statistical physics known as the Critical Point (CP) model has been put forth to account for equation (2) with a value $\gamma = 1/4$ [30]. In this model, it is assumed, based on seismic observation, that earthquakes occur at a constant rate in the seismic region, and that the mean rupture area $\mathcal{A}(\tau)$ of earthquakes occuring at time τ satisfies:

$$\mathcal{A}(\tau) \propto \frac{1}{(\tau_0 - \tau)}. \tag{3}$$

In turn, assumption (3) is justified by identifying the lengthscale $\mathcal{L}(\tau) \propto \mathcal{A}(\tau)^{1/2}$ with the correlation length of a statistical physical system described by Ginzburg-Landau mean field theory with a temperature parameter depending on τ [31]. Importantly, previous work has not explained why it is physically reasonable to describe statistics of seismic activation with thermal equilibrium statistical physics formalism, or precisely which statistical physics systems are relevant to modelling seismic activation. Therefore, the objective of this article is to advance the detailed mathematical description of the correspondence between nonlinear differential equation modelling and statistical physics modelling of seismic activation in a way that allows for testing of statistical physics model predictions against real seismic measurements.

The outline of the article is as follows. Section 2 introduces a sine-Gordon equation modelling earthquake fault dynamics during seismic activation and explains how inverse scattering theory of this equation implies a relation between statistics of earthquake occurrence during seismic activation and the eigenvalue statistics of a differential operator whose eigenfunctions characterize the distribution of stress in the seismic region. Section 3 uses this relation to model eigenvalue statistics with a 2D Coulomb Gas statistical physics model, and explains how this model accounts for deviation of earthquake occurrence statistics from Gutenberg-Richter statistics during seismic activation. Section 4 concludes by commenting on how the 2D Coulomb Gas statistical physics model implies the phase space dimension of a nonlinear dynamical system characterizing real time velocity model evolution in the seismic activation region is finite, and how this implication can be tested against real seismic measurements.

2. Materials and Methods

2.1. Fault Dynamics

In 1+1 spacetime dimensions, the differential equation:

$$A\partial_t^2 U(t,z) + B\partial_t U(t,z) - C\partial_z^2 U(t,z) = -\sin(U(t,z)/D). \tag{4}$$

has been used to model migration of earthquake hypocentres along earthquake faults in seismic regions over periods of time during which multiple earthquakes occur [7]. In this equation, t is real time, z coordinates the direction of earthquake hypocenter migration along an earthquake fault, $U(t,z)$ is the local displacement of elastic material across the earthquake fault, $A\partial_t^2 U(t,z)$ is the local inertial force acting on the fault material, $B\partial_z^2 U(t,z)$ is the local elastic restoring force acting on the fault material, and $C\partial_t U(t,z)$ and $\sin(U(t,z)/D)$ are local frictional force acting on the fault material attributed to periodic contact of the material with tectonic plates on either side of the fault. If the earthquake fault material has constant height h and shear modulus μ along the fault, a solution to equation (4) can be interpreted to describe propagation of shear stress acting on fault material.

Restricting focus to the case $C = 0$, it follows that with rescaling of t, z, and $U(t,z)$, each of the constants A, B, and D in equation (3) can be scaled to 1, so it is now assumed that each of these constants is 1. With this assumption, and definition of the matrices:

$$M = \begin{bmatrix} -i\omega & -\frac{1}{2}U_z(t,z) \\ \frac{1}{2}U_z(t,z) & i\omega \end{bmatrix}, \tag{5}$$

$$N = \frac{i}{4\omega}\begin{bmatrix} \cos U(t,z) & \sin U(t,z) \\ \sin U(t,z) & -\cos U(t,z) \end{bmatrix}, \tag{6}$$

for an arbitary complex number ω, the equation:

$$M_t - N_z + MN - NM = 0, \tag{7}$$

is equivalent to equation (3) [21]. This equivalence is of mathematical interest, because the associated linear system:

$$\begin{bmatrix} \Psi_1(t,z) \\ \Psi_2(t,z) \end{bmatrix} = M\begin{bmatrix} \Psi_1(t,z) \\ \Psi_2(t,z) \end{bmatrix}, \tag{8}$$

has an infinite set of left and right scattering (i.e. Jost) solutions $\Psi_{\lambda,L}(t,z)$ and $\Psi_{\lambda,R}(t,z)$, indexed by complex numbers λ, with asymptotics:

$$\Psi_{\lambda,L}(t,z) = \begin{bmatrix} 0 \\ e^{i\lambda z} \end{bmatrix},\ z \to \infty \tag{9}$$

$$\Psi_{\lambda,L}(t,z) = \begin{bmatrix} \frac{L(\lambda,t)e^{-i\lambda z}}{T(\lambda)} \\ \frac{e^{i\lambda z}}{T(\lambda)} \end{bmatrix},\ z \to -\infty, \tag{10}$$

and:

$$\Psi_{\lambda,R}(t,z) = \begin{bmatrix} e^{-i\lambda z} \\ 0 \end{bmatrix},\ z \to -\infty \tag{11}$$

$$\Psi_{\lambda,R}(t,z) = \begin{bmatrix} \frac{e^{-i\lambda z}}{T(\lambda)} \\ \frac{R(\lambda,t)e^{i\lambda z}}{T(\lambda)} \end{bmatrix},\ z \to \infty, \tag{12}$$

$$
\begin{tikzcd}
\mathbf{U}(0,z) \arrow[r] \arrow[d, "\text{sine-Gordon solution}"'] & \mathbf{U}_z(0,z) \arrow[r, "\text{direct scattering t=0}"] & \{R(\lambda,0),\{\lambda_j,c_j\}\} \arrow[d, "\text{time evolution}"] \\
\mathbf{U}(t,z) & \mathbf{U}_z(t,z) \arrow[l] & \{R(\lambda,t),\{\lambda_j,c_j\,e^{-it/(2\lambda_j)}\}\} \arrow[l, "\text{inverse scattering at t}"]
\end{tikzcd}
$$

Figure 2. Schematic of diagram of inverse scattering method applied to solve the sine-Gordon equation [1].

whose time evolution determines solutions to the original sine-Gordon equation via the inverse scattering method [1]. Moreover, linear system 8 also has a finite set of bound state solutions called Baker-Akhiezer functions.

Figure 2 is a diagram of how the inverse scattering method applies to solve the sine-Gordon equation in terms of solutions to linear system (8). In this diagram, real time evolution of an equation solution $U(t,z)$ is related by inverse scattering to real time evolution of the reflection coefficients $R(\lambda,t)$ and a finite set of complex numbers $\{c_j\}$ associated with eigenfrequencies $\{\lambda_j\}$ of bound state solutions to linear system (8). Note that in terms of inverse scattering theory, these bound states are in correspondence with zeroes of the function $T(\lambda)$, whereas resonant scattering states are in correspondence with zeros of the reflection coefficient $R(\lambda,t)$ at fixed values of t. Also, note that according to inverse scattering theory, the eigenfrequencies $\{\lambda_j\}$ have non-zero imaginary components, and are located symmetrically with respect to the real axis of the complex plane, so that the set of complex numbers $\{c_j(t)\}$ contain values whose magnitudes approach 0 and ∞ as t increases. This fact is important because it demonstrates that when one or more bound states exist whose magnitudes along the z-axis increase without bound as t increases, the distribution of stress in the seismic region is unstable, and the spatial form of the stress distribution is determined by the precise form of the bound state eigenfunctions.

To clarify physical interpretation of the Jost functions used by the inverse scattering method, note that in general, for a potential function $V(z)$ compactly supported along the z-axis, the operator:

$$-B\partial_z^2 + V(z), \tag{13}$$

has infinitely many eigenfunctions $\Psi(z)$ satisfying the elastic wave equation:

$$-B\partial_z^2\Psi(z) + V(z)\Psi(z) = E\Psi(z), \tag{14}$$

with positive real eigenvalues $E = \omega^2$, and finitely many bound state eigenfunctions $\Psi_j(z)$ with negative real eigenvalues $E_j < 0$. Consequently, a solution $\Psi(t,z)$ to the wave equation:

$$\partial_t^2\Psi(t,z) - B(\tau)\partial_z^2\Psi(t,z) + V(z)\Psi(t,z) = 0. \tag{15}$$

has a resonant scattering expansion of the form:

$$\begin{aligned}\Psi(t,z) = \sum_{j=1}^{N} e^{t\sqrt{-E_j}} a_j \Psi_{j,a}(z) \quad &+ \quad e^{-t\sqrt{-E_j}} b_j \Psi_{j,b}(z) \\ &+ \quad \sum_{\omega} e^{-it\omega} R_\omega \Psi_\omega(z),\end{aligned} \tag{16}$$

in which exponential growth and decay of the bound states determines the geometric form of the elastic perturbation $\Psi(t,z)$ over time. For example, if $V(z)$ is a potential well of height $V_0 > 0$ which is nonzero for $|z| \leq L$, and zero elsewhere, there exist finitely many bound state eigenfunctions $\Psi_j(z)$ which decay exponentially with increasing $|z|$:

$$\Psi_j(z) \propto e^{-k_j|z|}, \; |z| \to \infty \tag{17}$$

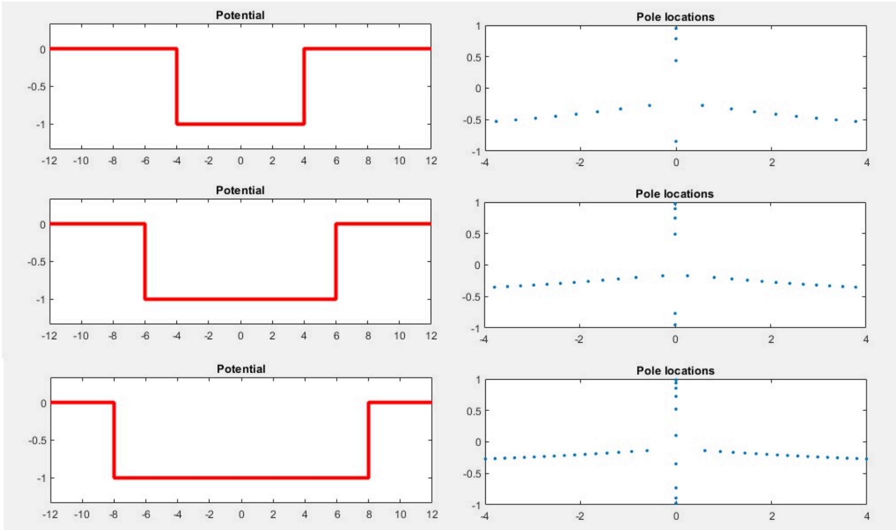

Figure 3. Plots of resonant frequency and bound state frequency locations for 3 square well potentials of increasing width.

for a discrete set of wavenumbers:

$$k_j = \sqrt{(V_0 + E_j)/B}, \tag{18}$$

whose inverse values determine characteristic length scales at which unstable growth of fault material displacement occurs across the earthquake fault. Figure 3 shows a plot of resonant and bound state frequency locations for 3 situations in which $-\frac{1}{B}V(z)$ is a square well potential of increasing width and fixed height.

The inverse scattering solution shown in Figure 2 also demonstrates that the bound state eigenfunction coefficients:

$$\mathcal{C}_j(t) \quad = \quad e^{-it/2\lambda_j} c_j, \tag{19}$$

satisfy the system of ordinary linear differential equations:

$$\dot{\mathcal{C}}_j(t) \quad = \quad (-i/2\lambda_j)\mathcal{C}_j(t), \tag{20}$$

implying unstable material displacement across the fault can be effectively described as the motion of a point in a dynamical system phase space $\mathcal{S}$ of real dimension $2N$, specified by a system of $2N$ ordinary differential equations, for which the $2N$ values of $-i/2\lambda_j$ are Lyapunov exponents.

2.2. Fault Dynamics to Statistical Physics

To relate the nonlinear differential equation description of fault dynamics (4) to a statistical physics model, start by introducing dependence of equation (7) on a parameter τ so that it reads:

$$M_t(\tau) - N_z(\tau) + M(\tau)N(\tau) - N(\tau)M(\tau) = 0, \tag{21}$$

where:

$$M(\tau) \quad = \quad \begin{bmatrix} -i\omega & -\frac{1}{2}U_z(t,z;\tau) \\ \frac{1}{2}U_z(t,z;\tau) & i\omega \end{bmatrix}, \tag{22}$$

$$N(\tau) \quad = \quad \frac{i}{4\omega}\begin{bmatrix} \cos U(t,z;\tau) & \sin U(t,z;\tau) \\ \sin U(t,z;\tau) & -\cos U(t,z;\tau) \end{bmatrix}. \tag{23}$$

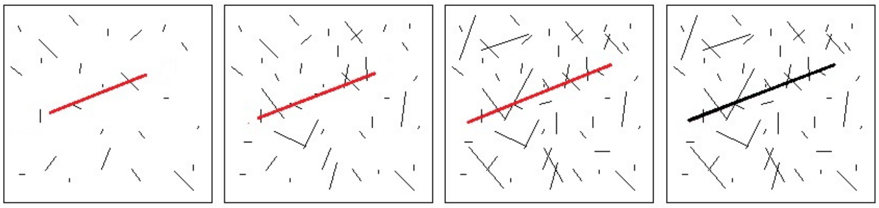

Figure 4. Schematic illustration of seismic activation in a 2D geometry at four different times τ in which each black line represents an earthquake fault along which rupture has occured, and each red line represents an earthquake fault along which shear stress is increasing prior to rupture at $\tau = \tau_0$.

The introduction of the parameter τ is the inverse scattering analog of introducing a parameter τ into the coefficients of elastic equation (15):

$$\partial_t^2 \Psi(t,z) - B(\tau)\partial_z^2 \Psi(t,z) + V(z;\tau)\Psi(t,z) = 0, \tag{24}$$

and interpreting τ as a real time parameter tracking the progression of seismic activation. Note that this interpretation implicitly assumes seismic activation and elastic wave propagation across the region undergoing seismic activation occur on sufficiently different timescales that it is reasonable to clock these processes with different real time parameters τ and t.

Now suppose material fracture along an earthquake fault caused by previous earthquakes during a period of seismic activation influences elastic scattering according to equation (15) with potential function $-\frac{1}{B}V(z;\tau)$ equal to a τ-dependent constant perturbed by random disorder over a compact interval of length $\mathcal{L}_0$ [19]. With this supposition, non-uniformity of the potential term in equation (24) at time τ accounts for scattering of elastic waves, and the maximum localization length $1/k_j$ of a bound state eigenfunction solving equation (24), henceforth denoted $\mathcal{L}(\tau)$, is interpretable as a length of fault material which is unstable to rupture. With reference to Figure 4, showing a schematic illustration of seismic activation in a 2D geometry at four different times τ, this length of unruptured fault material may be visualized as a line segment where shear stress exceeding some critical threshold has accumulated.

In 3 spatial dimensions, the previous discussion of stress localization in 1 spatial dimension can be generalized if it is assumed that shear waves propagating within a region of seismic activation at time τ are described by an elastic wave equation that is equivalent to equation (21) with matrices $M(\tau)$ and $N(\tau)$ determined by the P and S wave velocity model of the region at time τ. With this assumption, previous work simulating localization of stress in random fracture networks implies shear waves may be localized in 3 spatial dimensions at angular frequencies ω greater than a mobility edge frequency $\omega_c(\tau)$ [22]. Based on this previous work, it is now postulated that bound states of the τ-dependent inverse scattering problem have eigenfrequencies $\omega > \omega_c(\tau)$, are localized in space with maximum localization length $\mathcal{L}(\omega;\tau)$ satisfying:

$$\mathcal{L}(\omega;\tau) \propto (\omega - \omega_c(\tau))^{-1}, \tag{25}$$

and that the localization length of at least one such bound state is identifiable with the rupture length of the major earthquake occurring at time $\tau = \tau_0$.

To quantify these statements, it is now recalled that in both contexts of localization of seismic and electromagnetic waves in disordered elastic and dielectric materials, in analogy to the theory of Anderson localization, elastic and photonic states may be non-localized (i.e. extended) or localized at eigenfrequencies below or above a mobility edge frequency ω_c, as shown in Figure 5 where the leftmost dashed line is located at frequency ω_c [19,23]. It is also recalled that according to the scaling theory of Anderson localization, as a disorder parameter W in a 3D disordered electronic model Hamiltonian is increased from 0 to some critical value W_c, the distribution of normalized energy level spacings of non-localized states at a conduction band center changes from delta function (i.e. uniform level spacing) to Poisson as the two boundaries between localized and non-localized states (i.e. mobility edges) on opposite sides of the band center converge together [15,35]. More specifically, this theoretical statement is that as W is increased from $W \approx 0$ to $W \approx W_c$, the distribution of normalized energy level spacings at the band center is described by the Wigner surmise distribution:

$$P_\beta(s) = c_0\left(\frac{\pi s}{2}\right)^\beta e^{-\frac{1}{4}\beta\left(\frac{\pi s}{2}\right)^2 - \left(c_1 s - \frac{\beta}{4}\pi s\right)}, \tag{26}$$

with constants c_0 and c_1 determined by conditions:

$$\int_0^\infty P_\beta(s)ds = 1 \tag{27}$$

$$\int_0^\infty sP_\beta(s)ds = 1, \tag{28}$$

and a value of β which decreases from $\beta \approx \infty$ to $\beta \approx 0$. The relevance of this scaling theory to modelling seismic activation is now suggested by conjecturing that a Wigner surmise distribution with a τ-dependent value of β describes the density of elastic resonant scattering states in a neighborhood of $\omega_c(\tau)$, and that $\beta(\tau)$ decreases monotonically to a value $\beta(\tau_0)$ as $\tau \to \tau_0$.

3. Results

As initial evidence for the conjectured correspondence between major earthquakes and bound states of inverse scattering theory, first assume that during the time interval (τ_1, τ_2) the value of $\omega_c(\tau)$ is approximately constant, and that the density $\rho(\omega)$ of non-localized eigenstates in a neighborhood of the mobility edge shown in Figure 5 satisfies:

$$\rho(\omega) \propto |\omega - \omega_c(\tau)|^{\beta(\tau)}. \tag{29}$$

Furthermore, assume that the decay time of each non-localized resonant scattering is inversely proportional to a diffusion constant $\mathcal{D}(\omega)$ satisfying:

$$\mathcal{D}(\omega) \propto |\omega - \omega_c(\tau)|. \tag{30}$$

Then, if non-localized states correspond to seismic activation earthquakes with rupture length proportional to $1/(\omega - \omega_c(\tau))$ occurring during the time interval (τ_1, τ_2), and the state decay time corresponds to the recurrence time of earthquakes of the same magnitude, the number of earthquakes $\dot{N}_c$ with rupture length $\mathcal{L} > \mathcal{L}(\omega; \tau)$ occurring during the time interval satisfies:

$$\dot{N}_c \propto |\omega - \omega_c(\tau)|^{2+\beta(\tau)}, \tag{31}$$

from which it follows:

$$\log_{10} \dot{N}_c \approx \delta - (2 + \beta(\tau)) \log_{10} \mathcal{L}(\omega; \tau). \tag{32}$$

Therefore, noting the relation between seismic moment and Richter magnitude:

$$M_\mathcal{L} = \left(\log_{10}(M_0) - 9\right)/1.5, \tag{33}$$

and the definition of the seismic moment:

$$M_0 \propto \mathcal{L}(\omega; \tau_1)^2, \tag{34}$$

that equation (32) is equivalent to the Gutenberg-Richter relation:

$$\log_{10} \dot{N}_c = \bar{\delta} - 0.75(2 + \beta(\tau))M_\mathcal{L}. \tag{35}$$

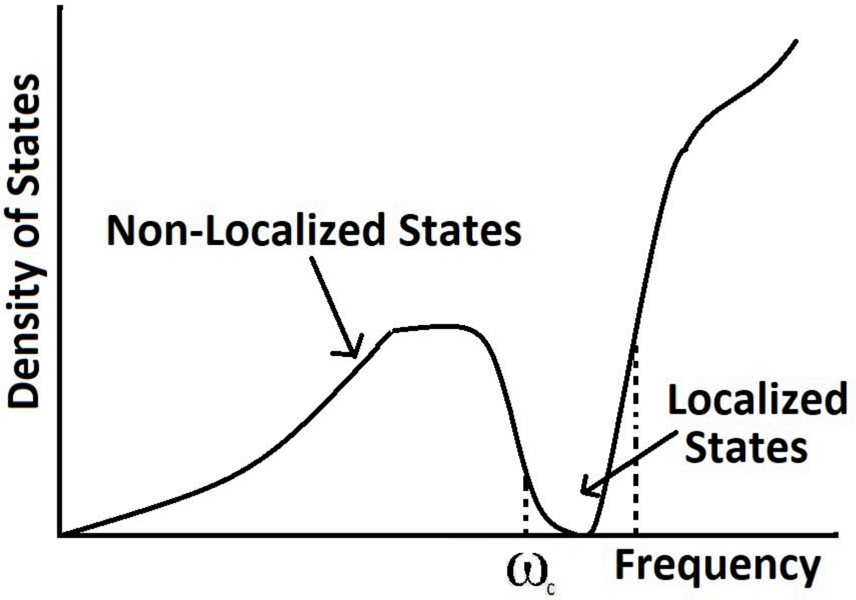

Figure 5. Photonic density of states in a disordered dielectric material [19]. Shaded region indicates frequencies associated with localized states.

Referring back to Figure 5, at times τ when the density of non-localized states is approximately constant so that $\beta(\tau) = 0$, the Gutenberg-Richter b-value is the physically reasonable value 1.5 [17,19].

If we now suppose that relation (30) is replaced with relation:

$$\mathcal{D}(\omega) \propto |\omega - \omega_c(\tau)|^{2/3}, \tag{36}$$

descriptive of critical slowing down of non-localized elastic state diffusion when $\omega \approx \omega_c(\tau)$, it follows that relation (31) is replaced with relation:

$$\dot{N}_c \propto |\omega - \omega_c(\tau)|^{5/3+\beta(\tau)}, \tag{37}$$

and the Gutenberg-Richter b-value in equation (35) is 1.25. Similarly, if the critical slowing down exponent in relation (36) is replaced with a value between 0 and 1, the Gutenberg-Richter b-value attains a value between 0.75 and 1.5. Therefore, if the density of non-localized photonic states $\rho(\omega)$ in Figure 5 is roughly constant except for a neighborhood of $\omega = \omega_c(\tau)$ where $\rho(\omega) \propto \omega^{\beta(\tau)}$, and the critical slowing down exponent decreases from 1 to a value between 0 and 1 as ω approaches $\omega_c(\tau)$ from below, it follows that the deviation from Gutenberg-Richter statistics shown in Figure 1 is accounted for by the physics of light localization and correspondence between non-localized photonic states near the mobility edge and seismic activation earthquakes.

Having provided initial evidence that Wigner-Dyson distributions are relevant to accounting for deviation of earthquake occurrence statistics from Gutenberg-Richter statistics during periods of seismic activation before a major earthquake, it is now further conjectured, in keeping with previous statistical physics models of seismic activation, that $\beta(\tau)$ can be regarded as a parameter in a τ-dependent 2D Coulomb gas statistical physics model whose parameters at different values of τ are related by renormalization group flow [14]. In part, this conjecture is motivated by previous work demonstrating the porous medium equation, a nonlinear diffusion equation in 1 spatial dimension, is equivalent to a renormalization group flow equation for a disorder potential in a statistical physics model, although it remains unclear whether or not a nonlinear differential equation descriptive of earthquake fault dynamics can be similarly derived as a renormalization group flow equation [2,8].

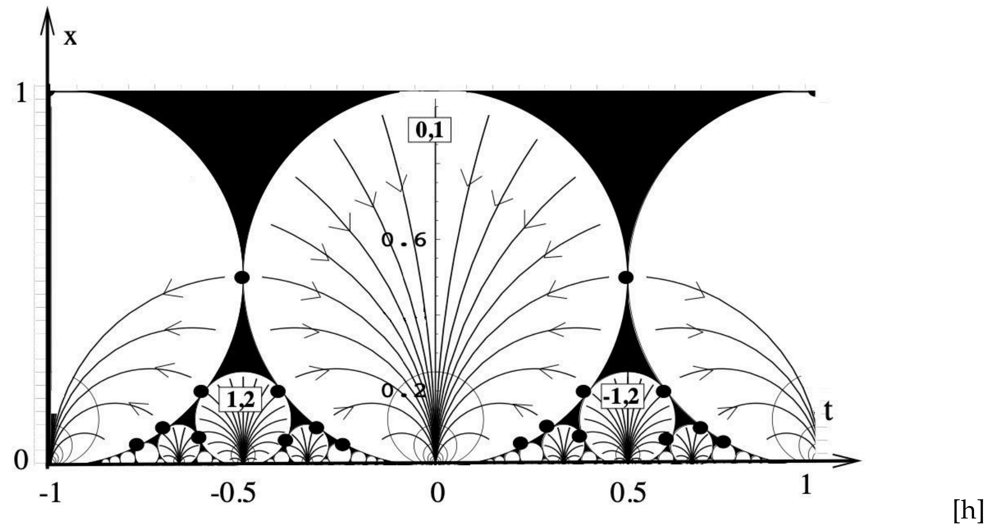

Figure 6. Phase diagram of 2D Coulomb gas with renormalization group flow indicated by arrows and KT critical points identified by circle tangencies [9].

A phase diagram of a 2D Coulomb gas with a renormalization group flow indicated by arrows is shown in Figure 6. In this diagram, different vaues of the flow coordinate 't' equate to $\beta(\tau)$ at different values of τ in such a way that $\beta(\tau_0)$ is the horizontal coordinate of a point of tangency between two of the Ford circles. It should also be noted that this diagram corresponds to the $M = 1$ description of a more general 2D Coulomb gas statistical physics model defined by a field theory with M complex fields ϕ whose domain of definition is a 2D complex plane, and whose amplitudes quantify the density of eigenvalues of a differential operator at different complex frequencies [13].

To elaborate on this identification of a statistical physics model relevant to modelling seismic activation, suppose that as a result of stress accumulation in the Earth's subsurface during seismic activation, the elastic potential function $V(x, y, z; \tau)$ descriptive of a seismic region's seismic velocity model oscillates around its average value at each point in space at a set of characteristic frequencies $Re(\omega_j) < \omega_c(\tau)$, where each complex frequency ω_j is an inverse scattering theory resonant frequency [29]. Next, suppose random variation of the seismic region elastic velocity model during activation can be approximated by attributing it to oscillation at a finite number M of these eigenfrequencies ω_j. With this supposition, the M τ-dependent complex eigenfrequencies of the shear stress eigenfunctions define a torus of real dimension $2M$ identified by a point in a Siegel moduli space $\mathcal{M}$, and τ-dependence of the complex frequencies is determined by motion of a point in the moduli space. It is this motion which is described by the renormalization group flow of a 2D Coulomb gas model near its critical point, assuming the model has M fields ϕ_j and coefficients coordinating points of $\mathcal{M}$ [9,11,40]. In passing, the possibility that correlation functions of the statistical field theory satisfying differential equations of order N describe N bound states of shear stress nucleation in the Earth's subsurface before the moment of earthquake rupture is noted [39].

4. Discussion

Previous work has identified predicting the time of occurrence of major earthquakes as a possible application of statistical physics models of seismic activation, but this application has not yet been realized [5]. In more recent times, earthquake early warning algorithms such as FinDer and Virtual Seismologist have been developed which can in principle use previous earthquake occurrence statistics as input, and most recently, artificial intelligence algorithms such as QuakeGPT have been developed for predicting the occurrence of major earthquakes using seismic event records created with stochastic simulators as training data [4,32]. Therefore, a practical applied science goal for the statistical physics model presented in this article appears to be improving the predictive performance of one or more of these existing earthquake early warning algorithms by appropriately modifying their earthquake occurrence statistical inputs, acknowledging that preliminary tests of the model's validity against real seismic data must be passed before achieving this application objective can be considered a realistic possibility.

From a geophysical testing point of view, if it is true that the growth of unstable stress modes within the Earth during seismic activation are determined by statistical physics renormalization group flow mathematics, and, as a result, a nonlinear dynamical system of phase space dimension N characterizes the nucleation of shear stress in a seismic region preceding a major earthquake, a geophysical signal processing technique known as singular spectrum analysis should apply to determine this phase space dimension [6]. Therefore, it is suggested that coda wave interferometry measurements of relative changes in seismic surface wave and/or body wave velocity be performed between pairs of seismic stations in a seismic region over a duration of time during which seismic activation is known to have occurred, and used as input to a time domain multichannel singular spectrum analysis algorithm [25]. The number of channels of this algorithm would equate to the number of station pairs, and the number of singular values output by the algorithm in different time windows preceding occurrence of a major earthquake should provide some indication of a finite value for N if the statistical physics model of seismic activation is correct in principle. With reference to previous geophysical application of singular spectrum analysis, performed in the frequency domain, the signal processing algorithm suggested here is different in that it should be carried out in the time domain τ rather than the frequency domain [33].

In conclusion, work towards improving current earthquake early warning systems can proceed in two directions. Firstly, as an initial check on whether or not the statistical physics modelling approach presented here could be of practical utility, work can be done to determine whether or not changes of the Earth's elastic velocity model preceding major earthquakes, as determined by coda wave interferometry, can be processed to extract an integer identifiable as the phase space dimension of a nonlinear dynamical system. Secondly, work can be done to elaborate upon the statistical physics mathematical model of seismic activation presented in this article to determine other tests of its scientific validity and potential for practical application.

Funding: This research received no external funding.

Acknowledgments: Thanks to Dr. Girish Nivarti and Professor Richard Froese for their willingness to entertain discussions about the content of the article.

Conflicts of Interest: The authors declare no conflicts of interest.

References

1. Aktosun T, Demontis F, F Van der Mee C. Exact solutions to the sine-Gordon equation. Journal of Mathematical Physics. 51(12).
2. Balog I, Carpentier D, Fedorenko AA. Disorder-driven quantum transition in relativistic semimetals: functional renormalization via the porous medium equation. Physical review letters. 2018 121(16):166402
3. Ben-Zion Y, Lyakhovsky V (2002) Accelerated seismic release and related aspects of seismicity patterns on earthquake faults. Earthquake processes: Physical modelling, numerical simulation and data analysis Part II :2385–2412
4. Böse M, Andrews J, Hartog R, Felizardo C. Performance and next-generation development of the finite-fault rupture detector (FinDer) within the United States West Coast ShakeAlert warning system. Bulletin of the Seismological Society of America. 2023 Apr 1;113(2):648–63
5. Bowman D, Ouillon G, Sammis C, Sornette A, Sornette D (1998) An observational test of the critical earthquake concept. Journal of Geophysical Research: Solid Earth 103(B10):24359–24372
6. Broomhead D S, King G P (1986) Extracting qualitative dynamics from experimental data. Physica D: Nonlinear Phenomena 20(2-3):217–236
7. Bykov V G (2001) Solitary waves on a crustal fault. Volcanology and Seismology 22(6):651–661.
8. Carlson J M, Langer J S, Shaw B E (1994) Dynamics of earthquake faults. Reviews of Modern Physics 66(2):657
9. Carpentier D (1999) Renormalization of modular invariant Coulomb gas and sine-Gordon theories, and the quantum Hall flow diagram. Journal of Physics A: Mathematical and General 32(21):3865

10. Cooper NR, Halperin BI, Hu CK, Ruzin IM (1997). Statistical properties of the low-temperature conductance peak heights for Corbino disks in the quantum Hall regime. Physical Review B 55(7):4551
11. Dubrovin B, Yang D (2020) Matrix resolvent and the discrete KdV hierarchy. Communications in Mathematical Physics 377:1823–1852
12. Dyatlov S, Zworski M (2019) Mathematical theory of scattering resonances, volume 200. American Mathematical Soc.
13. Dyson FJ, Mehta ML (1963) Statistical theory of the energy levels of complex systems. iv. Journal of Mathematical Physics 4(5):701–712
14. Goldenfeld N (2018). Lectures on phase transitions and the renormalization group. CRC Press.
15. Hofstetter E, Schreiber M (1993) Statistical properties of the eigenvalue spectrum of the three-dimensional Anderson Hamiltonian. Physical Review B 48(23):16979
16. Imada M, Fujimori A, Tokura Y (1998) Metal-insulator transitions. Reviews of modern physics 70(4): 1039.
17. Ito R, Kaneko Y (2023). Physical Mechanism for a Temporal Decrease of the Gutenberg-Richter b-Value Prior to a Large Earthquake. Journal of Geophysical Research: Solid Earth 128(12):e2023JB027413
18. Jensen HJ (2003) Lecture Notes on Kosterlitz-Thouless Transition in the XY Model. Imperial College Lectures 9
19. John S. Localization of light. Physics Today. 1991 May 1;44(5):32–40.
20. Johnston AC, Kanter LR, Coppersmith KJ, Cornell CA (1994) The earthquakes of stable continental regions. volume 1, assessment of large earthquake potential, final report. Electric Power Research Inst.(EPRI), Palo Alto, CA (United States)
21. Khan BA, Chatterjee S, Sekh GA, Talukdar B (2020) Integrable systems: From the inverse spectral transform to zero curvature condition. arXiv preprint arXiv:2012.03456
22. Lei Q, Sornette D (2022) Anderson localization and reentrant delocalization of tensorial elastic waves in two-dimensional fractured media. Europhys. Letters 136(3): 1–7
23. Markos P (2006) Numerical analysis of the Anderson localization. arXiv preprint cond-mat/0609580
24. Md BY, Giurgiutiu V (2016) Using the gauge condition to simplify the elastodynamic analysis of guided wave propagation. Incas Bulletin. 8(3):11.
25. Merrill RJ, Bostock MG, Peacock SM, Chapman DS (2023) Optimal multichannel stretch factors for estimating changes in seismic velocity: Application to the 2012 M_w 7.8 Haida Gwaii earthquake. Bulletin of the Seismological Society of America 113(3):1077–1090
26. Newman WI, Turcotte DL, Gabrielov AM (1995) Log-periodic behavior of a hierarchical failure model with applications to precursory seismic activation. Physical Review E 52(5):4827
27. Papazachos C, Papazachos B (2001) Precursory accelerated Benioff strain in the Aegean area
28. Reches ZE (1999) Mechanisms of slip nucleation during earthquakes. Earth and Planetary Science Letters. Jul 30;170(4):475–86
29. Ruelle D, Takens F (1971) On the nature of turbulence. Les rencontres physiciens-mathématiciens de Strasbourg-RCP25 12:1–44.
30. Rundle JB, Klein W, Turcotte DL, Malamud BD (2001) Precursory seismic activation and critical-point phenomena. Microscopic and Macroscopic Simulation: Towards Predictive Modelling of the Earthquake Process 2165–2182
31. Rundle JB, Turcotte DL, Shcherbakov R, Klein W, Sammis C (2003) Statistical physics approach to understanding the multiscale dynamics of earthquake fault systems. Reviews of Geophysics 41(4)
32. Rundle JB, Fox G, Donnellan A, Ludwig IG (2024) Nowcasting Earthquakes with QuakeGPT: Methods and First Results. arXiv e-prints. 2024 Jun:arXiv-2406
33. Sacchi M (2009) FX singular spectrum analysis. Cspg Cseg Cwls Convention 392–395
34. Saleur H, Sammis C, Sornette D (1996) Renormalization group theory of earthquakes. Nonlinear Processes in Geophysics 3(2):102–109
35. Soerensen M, Schneider T (1991) Level-spacing statistics for the Anderson model in one and two dimensions. Physik B Condensed Matter 82(1):115–119
36. Sornette D (1989) Acoustic waves in random media: II Coherent effects and strong disorder regime, Acustica 67(4):251–265
37. Takahashi DA (2023) Multi-soliton solutions of the sine-Gordon equation with elliptic-function background. arXiv preprint arXiv:2301.08705. 2023 Jan 20.
38. Tzanis A, Vllianatos F (2003) Distributed power-law seismicity changes and crustal deformation in the SW Hellenic ARC. Natural Hazards and Earth System Sciences 3(3/4):179–195
39. Varchenko A (1990) Multidimensional hypergeometric functions in conformal field theory, algebraic K-theory, algebraic geometry. In Proceedings of the International Congress of Mathematicians 1:281–300
40. Zabrodin A (2010) Canonical and grand canonical partition functions of Dyson gases as tau-functions of integrable hierarchies and their fermionic realization. Complex Analysis and Operator Theory 4:497–514
41. Zuo Z, Yin S, Cao X, Zhong F (2021) Scaling theory of the Kosterlitz-Thouless phase transition. Physical Review B 104(21):214108